Available online at www.sciencedirect.com
ScienceDirect
Composites: Part B 39 (2008) 202–208
composites Part B: engineering
www.elsevier.com/locate/compositesb

Bending buckling of single-walled carbon nanotubes by atomic-scale finite element

X. Guo [a], A.Y.T. Leung [a,*], X.Q. He [a], H. Jiang [b], Y. Huang [c]

[a] Department of Building and Construction, City University of Hong Kong, Hong Kong
[b] Department of Mechanical and Aerospace Engineering, Arizona State University, Tempe, AZ 85287-6106, USA
[c] Department of Mechanical and Industrial Engineering, University of Illinois at Urbana-Champaign, 1206 West Green Street, Urbana, IL 61801, USA

Available online 12 March 2007

Abstract

This paper employs the atomic-scale finite element method to study bending buckling of single-walled carbon nanotubes (SWNTs). As the bending angle increases, kinks will appear and the morphology of the SWNT will change abruptly. The (15,0) SWNT changes into a one-kinked structure, and finally contains two kinks; while the (10,0) SWNT changes into a one-kinked structure, then into a two-kinked one, and finally contains three kinks. Strain energy grows initially as a quadratic function of bending angle, then increases gradually slowly, and finally changes approximately linearly. The energy releases suddenly at morphology bifurcations and the amount depends on degree of morphology change. The simulation shows that the appearance of kinks associated with the large deformation nearby reduces the slope of the strain energy curve in the post-buckling stages and hence increases the flexibility of the SWNTs.

Keywords: A. Nano-structures; B. Buckling; C. Computational modelling; Morphology change

1. Introduction

Examining slices of carbon nanotubes (CNTs) embedded within a polymeric film by transmission electron microscopy, Lourie et al. [1] reported that bent CNTs collapse to form kinks. Hadjiev et al. [2] demonstrated CNTs buckling and debonding in single-walled CNT (SWNT)/epoxy nano-composites, by means of Raman spectroscopy and transmission electron microscopy. Buckling of CNTs is very important to the strength and failure of CNTs-based composites. To investigate bending buckling of the CNTs, theoretical research has been carried out in the last decade. In general, the important theoretical methods include molecular dynamics (MD) and continuum mechanics. Using MD, Yakobson et al. [3] found that a SWNT switches into a kink pattern beyond critical bending angle. Iijima et al. [4] performed MD simulation and achieved kinked structure at high bending angles. Shibutani and Ogata [5] presented MD study on the bending of a cantilevered SWNT loaded by a follower lateral force at the free end and found that it exhibited local buckling near the fixed end. Even for the axial compression and tension of CNTs, the MD simulation is so computationally expensive that they are currently limited to very small length and time scales [6–8]. Besides the great computational effort, the MD simulation on the bending buckling of CNTs involves other difficulties such as realization of moment on an atomistic system and large deformation near the kinks. Thus, the MD simulation on bending buckling is limited comparing with that on axial deformation. There is some investigation based on continuum mechanics to study the bending buckling of CNTs. Pantano et al. [9] presented a shell model and studied wrinkling of multi-walled CNTs (MWNTs). Wang and Wang [10] used theory of finite elasticity deformation to simulate wavelike configuration of the bent CNTs. Vodenitcharova and Zhang [11] studied the bending of a SWNT assuming moderate bending angles. In their model, the pre-buckling response was modeled using the continuum mechanics accounting for the ovalization of the

* Corresponding author. Tel.: +852 27887600; fax: +852 27887612.
E-mail address: bcaleung@cityu.edu.hk (A.Y.T. Leung).

1359-8368/$ - see front matter © 2007 Elsevier Ltd. All rights reserved.
doi:10.1016/j.compositesb.2007.02.025

cross-section and the post-buckling behavior was characterized by the development of an elastic kink. Wang et al. [12] used elastic beam theory to study bending buckling of double-walled CNTs, modeling the intra-tube interaction energy with the bending deformation energy. In the above continuum models, inter-atomic potential was not employed and multi-body interactions could not be considered accurately, so the behavior of discrete atom and concrete configuration of CNTs could hardly be achieved.

Liu et al. [13,14] proposed an atomic-scale finite element method. Using inter-atomic potential to consider the multi-body interactions, it is as accurate as molecular mechanics simulation and is much faster than the conjugate gradient method. The present authors [15] employed it to study axial buckling of CNTs, and found that in the post-buckling stages the strain energy increases approximately piecewise linearly with the strain. Further, the present paper employs it to study the bending buckling of SWNTs. (15,0) and (10,0) SWNTs are taken as examples. When the bending angle is large enough, a kink is initiated, morphology of the SWNT changes abruptly, and strain energy has a drop. After that, the strain energy increases approximately piecewise linearly with respect to the bending angle and more kinks appear. The morphologies of kinked SWNT are presented in detail. Because the kink can serve as hinge, SWNT can be bent to a very large angle and processes excellent flexibility.

2. Simulation procedure on bending buckling of SWNTs

For a straight SWNT in equilibrium, take the center of the circle formed by the left boundary atoms as origin O, the longitudinal direction of SWNT as z axis, and the cross-section as x–y plane. The plane where the boundary atoms lie is called the boundary plane, and the angle made by the two boundary planes is called bending angle. Without loss of generality, bending behavior of SWNT in the x–z plane is studied. The bent SWNT with bending angle 2θ is shown in Fig. 1. Note that the origin O is fixed, while the point P measuring the bending angle changes with the deformation.

Before the increment step i, the coordinate of the atom is $(x(i), y(i), z(i))$, and the bending angle is $2\theta(i)$. To realize the bending angle increment $2\Delta_i$ in step i, two sub-steps are needed. In the first sub-step, only mathematical transformations are performed to make the boundary planes rotate and move toward each other gradually. For the left boundary atoms, the following transformation is performed:

$$z(i+1) = z(i) + \frac{x(i)}{\cos(\theta(i))}\sin(\theta(i)) - \frac{x(i)}{\cos(\theta(i))}\sin(\theta(i)+\Delta_i) + t(i) \tag{1}$$

$$x(i+1) = \frac{x(i)}{\cos(\theta(i))}\cos(\theta(i)+\Delta_i) \tag{2}$$

For the right boundary atoms, the following transformation is performed:

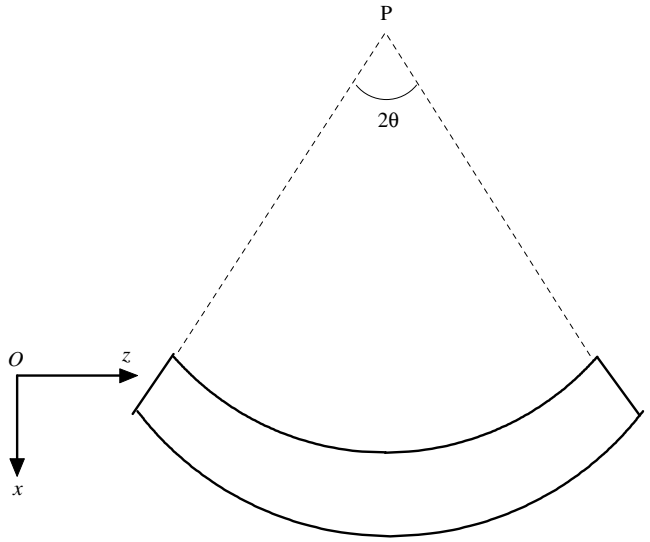

Fig. 1. The sketch of a bent SWNT with bending angle 2θ.

$$z(i+1) = z(i) - \frac{x(i)}{\cos(\theta(i))}\sin(\theta(i)) + \frac{x(i)}{\cos(\theta(i))}\sin(\theta(i)+\Delta_i) - t(i) \tag{3}$$

$$x(i+1) = \frac{x(i)}{\cos(\theta(i))}\cos(\theta(i)+\Delta_i) \tag{4}$$

where $t(i)$ is the given z displacement of two boundary planes to consider their overall translational movement toward each other during large deformation. For a small bending angle, $t(i)$ can be taken as zero. When the bending angle increases, it can increase gradually. $y(i)$ is not involved in the above transformations. Except the boundary atoms, the others are kept fixed in this sub-step.

In the second sub-step, the transformed configuration in the first sub-step is taken as an initial configuration, and the atomic-scale finite element simulation for the whole atomistic system is performed. The covalent bonds among the atoms are modeled according to Brenner et al.'s "second generation" empirical potential [16]. Each atomic-scale finite element consists of ten atoms including the central carbon atom, the three nearest-neighboring atoms and the six second nearest-neighboring atoms. A schematic diagram of the atomic-scale finite element, the associated element stiffness matrix and the non-equilibrium force vector are therein [13,14]. The element captures the interactions among the central atom and the other atoms. The number of non-zero entries in the global stiffness matrix K is of the order N, the number of atoms involved in the simulation. All calculation is performed by ABAQUS via its UEL subroutine [17]. In the simulation, keep $x(i)$ and $z(i)$ of the boundary atoms fixed while relax the other atoms to find a new equilibrium configuration. One has to fix $y(i)$ of at least one boundary atom in the simulation to avoid global rigid-body movement of the SWNT. Here, $y(i)$ of a

boundary atom in the left boundary plane is fixed, while $y(i)$ of other boundary atoms are free in this sub-step.

In this sub-step, the initial configuration may be far from the final equilibrium configuration, so the global stiffness matrix K may lose positive definiteness. When K is no longer positive definite, it is replaced by $K^* = K + \alpha I$, where I is the identity matrix and α is a positive number to ensure the positive definiteness of K^*. A trial configuration is achieved by the simulation. Based on the trial configuration, a new smaller α is chosen to ensure the positive definiteness of the new K^*. We perform the simulation and replace the stiffness matrix repeatedly. The calculation converges finally without replacing the stiffness matrix and the new equilibrium configuration is achieved. The repeated replacement of stiffness matrix is an efficient approach to obtain the modified initial configuration, and the final modified initial configuration may lead to a converged result. Note that in the final step the replacement is not performed (α is 0), so the final results will be the equilibrium configuration of the original system.

For the new equilibrium configuration, the coordinates of atoms are denoted as $(x(i+1), y(i+1), z(i+1))$, and next increment step $i+1$ can be performed. With the bending angle increasing, kinks will appear and the morphology of SWNT will change abruptly at certain bending angles, which are the critical angles for bending buckling.

3. Numerical results

First, the bending buckling of a (15,0) SWNT with a length of 8.35 nm is studied. Here the angle increment Δ_i and the controlled movement of the boundary plane $t(i)$ are given as follows. If the bending angle is less than 0.4 (radian), Δ_i is taken as a comparatively larger value, 0.05; otherwise, it is always taken as 0.01. If the bending angle is less than 0.4, $t(i)$ is taken as 0; if the bending angle is between 0.4 and 0.6, it increases from 0.001 to 0.01 linearly; otherwise, it is taken as 0.01 constantly. The above values are chosen to make two ends of the bent SWNT approach approximate 20–40% of its initial length when the bending angle reaches a large value such as 2.0.

The total strain energy is calculated as the difference of the energy in the bent and un-bent system as a function of bending angle as shown in Fig. 2. The morphologies of the (15,0) SWNT in the x–z plane are presented in Fig. 3 [18]. At small bending angle, it deforms linearly as shown in Fig. 3a, and the strain energy grows quadratically with respect to the bending angle as shown in Fig. 2. Due to the controlled movement of the two boundary planes, the increment of the strain energy slows down. At the critical bending angle of 0.64, one kink appears, as shown in Fig. 3b. From 0.624 to 0.660, a detailed simulation is made by taking the angle increment Δ_i and the controlled movement of the boundary plane $t(i)$ as one fifth of the normal values. Δ_i is taken as 0.002 and $t(i)$ is taken as 0.002. The results are presented in the insert of Fig. 2. It is found that the strain energy decreases from 25.65 eV when the bending angle is 0.636 to 25.17 eV when the bending angle is 0.640. The first critical bending angle 0.640 corresponds to 36.7°, while in the MD simulation of Iijima et al. [4] for the same (15,0) SWNT, it is approximately 30°, reasonably well in agreement with the present critical angle. When the bending angle increases, the kink becomes larger gradually as seen in Fig. 3d and e, and the strain energy increases approximately linearly till the second critical bending angle of 1.20. From 1.184 to 1.220, a detailed simulation is made by taking the angle increment and the controlled moving of the boundary plane as one fifth of the normal values. The results are also presented in the insert of Fig. 2. It is found that the strain energy decreases from 58.38 eV when the bending angle is 1.196 to 54.18 eV when the bending angle is 1.200. Comparing with the first one, this energy release reaches 7.2% and is much more obvious in Fig. 2. After the second buckling, the bent SWNT changes into a two-kinked structure, as shown in Fig. 3f. With further increasing of bending angle, two kinks become larger and larger, as shown in Fig. 3g–m. Because y coordinate of a boundary atom is fixed, the configuration of SWNT does not possess the left–right symmetry strictly.

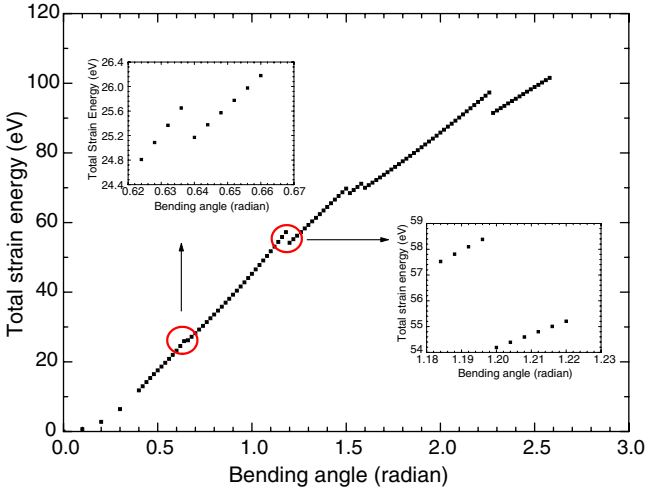

Fig. 2. The curve of total strain energy for the (15,0) SWNT versus the bending angle.

As a next example, consider the bending buckling of a (10,0) SWNT with a length of 8.33 nm. The angle increment and the controlled movement of the boundary planes are the same with those for the (15,0) SWNT. The total strain energy versus the bending angle is shown in Fig. 4. Its morphologies in the x–z plane are presented in Fig. 5 [18]. At small bending angle, it deforms linearly as shown in the Fig. 5a, and the strain energy increases as a quadratic function of the bending angle, as shown in Fig. 4. Then the increasing of the strain energy slows down. At the critical bending angle of 1.04, it buckles and contains one kink as shown in Fig. 5b. When the bending angle increases, the kink becomes larger gradually in Fig. 5c–f. In Fig. 4, the strain energy increases approximately linearly till the second critical bending angle of 1.82. In the second

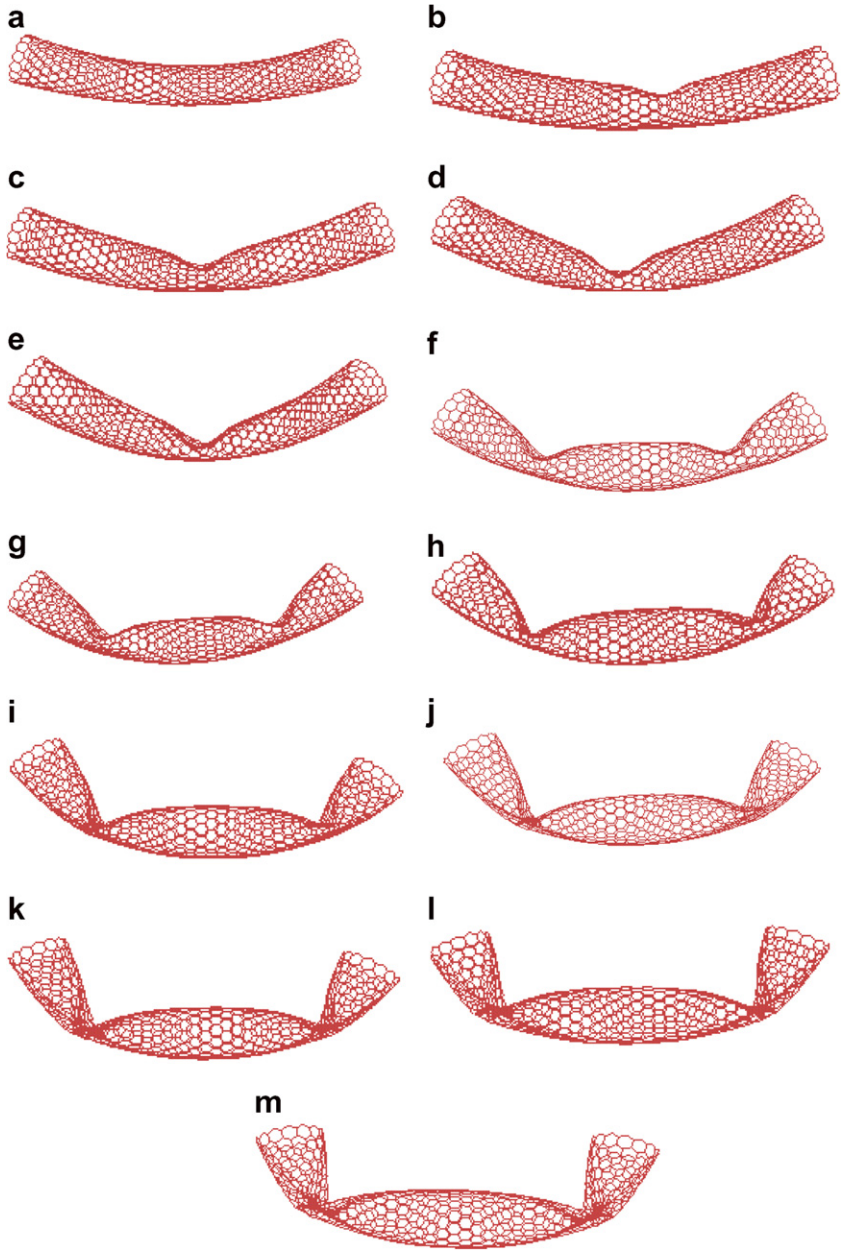

Fig. 3. The morphologies of the (15,0) SWNT in bending: (a) bending angle of 0.62, (b) bending angle of 0.64, (c) bending angle of 0.80, (d) bending angle of 1.00, (e) bending angle of 1.18, (f) bending angle of 1.20, (g) bending angle of 1.40, (h) bending angle of 1.60, (i) bending angle of 1.80, (j) bending angle of 2.00, (k) bending angle of 2.20, (l) bending angle of 2.40 and (m) bending angle of 2.60.

buckling, the strain energy has a small drop to another straight line, and the one-kinked SWNT changes into a two-kinked structure, as shown in Fig. 5g. The first kink lies in the center and still very large, and the second kink lies approximately one sixth length away from the end. When the bending angle increases to the third critical bending angle of 1.92, the two-kinked SWNT changes into a three-kinked structure, as shown in Fig. 5h. The third kink lies approximately in one sixth length away from the other end. With further increasing of the bending angle, the left and right kinks become larger and larger, as shown in Fig. 5i–l.

4. Discussion and conclusion

When the bent SWNT first buckles, Yakobson et al. [3], Iijima et al. [4], and Vodenitcharova and Zhang [11] showed there is only a small energy release. In the present studies, there are always small energy releases in the first buckling, which is consistent with their research [3,4,11]. For the second buckling of (15,0) SWNT, there is a comparatively large energy release; while for the second and third buckling of (10,0) SWNT, there are only small energy releases. The amount of energy release depends on the degree of morphology change during buckling. For the

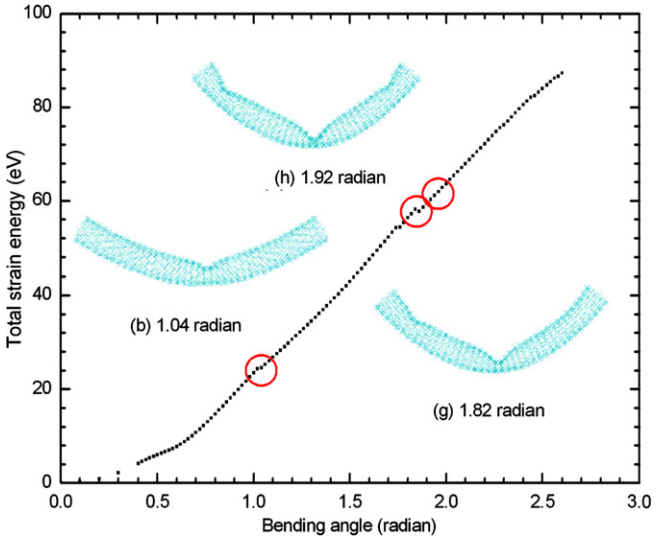

Fig. 4. The curve of total strain energy for the (10,0) SWNT versus the bending angle.

(15,0) SWNT, when the bending angle increases from 1.18 to 1.20, the SWNT containing a kink at its center changes into that containing two kinks at its two sides as shown in Fig. 3e and f. A clear energy release accompanies with this large change of the configuration as shown in Fig. 2. For the (10,0) SWNT, when the bending angle increases from 1.80 to 1.82, the first kink still lies in the center, a small kink appear on one side of the SWNT as shown in Fig. 5f and g. When the bending angle further increases to 1.92, the first and second kinks still lie there, the third one appears on the other side of the SWNT as shown in Fig. 5h. In the above two buckling phenomena, the configurations of the (10,0) SWNT only have small changes, so no large energy release accompanies them as shown in Fig. 4.

In Figs. 2 and 4, in each post-buckling stage, the strain energy changes approximately piecewise linearly with the bending angle, in agreement with Yakobson et al. [3], Iijima et al. [4] and Vodenitcharova and Zhang [11]. For each curve segment, the average slope is smaller than that of the former one. The above is similar with our study on axial buckling of SWNTs, where in each post-buckling stage the strain energy changes approximately linearly with the strain [15].

The (15,0) and (10,0) SWNTs studied here have almost the same length, so the latter has a comparatively larger aspect ratio. The (10,0) SWNT has a comparatively larger first critical angle, which can be explained as follows. For a beam in pure bending with small amplitude, the central line has no axial strain, and the same bending angle represents the same curvature. If the present cases are similar to those of continuum mechanics, the (10,0) SWNT with smaller radius would have the smaller maximum compressive strain, so its critical bending angle is comparatively larger.

Here their bending angle can reach 2.6, at which angle the (15,0) SWNT contains two kinks and the (10,0) SWNT contains three kinks. They possess good flexibility, which is consistent with the available experimental research [1,19,20]. It is reasonable that the SWNT with a larger aspect ratio has more complicated global structure. The phenomenon that SWNTs possess good flexibility due to bending buckling is similar with the recent experimental founding that the freestanding films of vertically aligned CNTs exhibit super-compressible foam-like behavior due to axial compressive buckling [21]. The two kinks in Fig. 3i–m for the (15,0) SWNT and the central kink in Fig. 5i–l for the (10,0) SWNT corresponds to hinges, and are similar to the available MD simulation [3,4] and experimental research [20]. In Iijima et al. [4], when the bending angle increases from 30° to 120°, the strain energy increases continuously and it always contains one kink; while in the present simulation, the strain energy has several releases and it contains two kinks finally. Here, Eqs. (1)–(4) are employed to realize the rotation of the ends of SWNT, while in Iijima et al., the details on how to realize the moment were not explicitly expressed, and the difference in those details may accumulate and lead to large difference in the final configuration. Another important reason may be in the employed potential functional. The Brenner's empirical potential [22] was employed in MD simulation of Iijima et al. [4], while the Brenner et al.'s "second generation" empirical potential [16] is employed in the present simulation. The latter includes both improved analytic functions for the inter-atomic interactions as well as an expanded fitting database.

Because SWNTs are studied here, the kinks can become very large. While for the MWNTs, due to the interactions of different layers, the kinks can not become comparatively large, and rippled structure, which can be considered as a series of small kinks, appears in the compressive side of the bent MWNTs [1,9,10,23].

In conclusion, the atomic-scale finite element method is employed to study the bending buckling of the SWNTs in this paper. For the (15,0) SWNT, a kink is initiated at the first critical angle and it changes into a two-kinked structure at the second critical angle. For the (10,0) SWNT, a kink is initiated at the first critical angle, it changes into a two-kinked structure at the second critical angle, and it changes into a three-kinked structure at the third critical angle. After buckling, the strain energy changes approximately piecewise linearly with the bending angle, and the slope of each segment is smaller than that in the former stage. Physically, smaller slope implies more flexible after each morphology change. The kinks can become very large and correspond to hinges. The present simulation shows that SWNT has very good flexibility and is consistent with the available experimental research. The buckling leading to the large deformation and the strain energy curve having smaller slope in the post-buckling stages, are the intrinsic reason that SWNTs have good flexibility.

The post-buckling behaviors of the (15,0) and (10,0) SWNTs differ a lot, especially their final morphologies. Generally speaking, the bending bucking is related to the critical local curvature, as shown in Yakobson et al. [3]

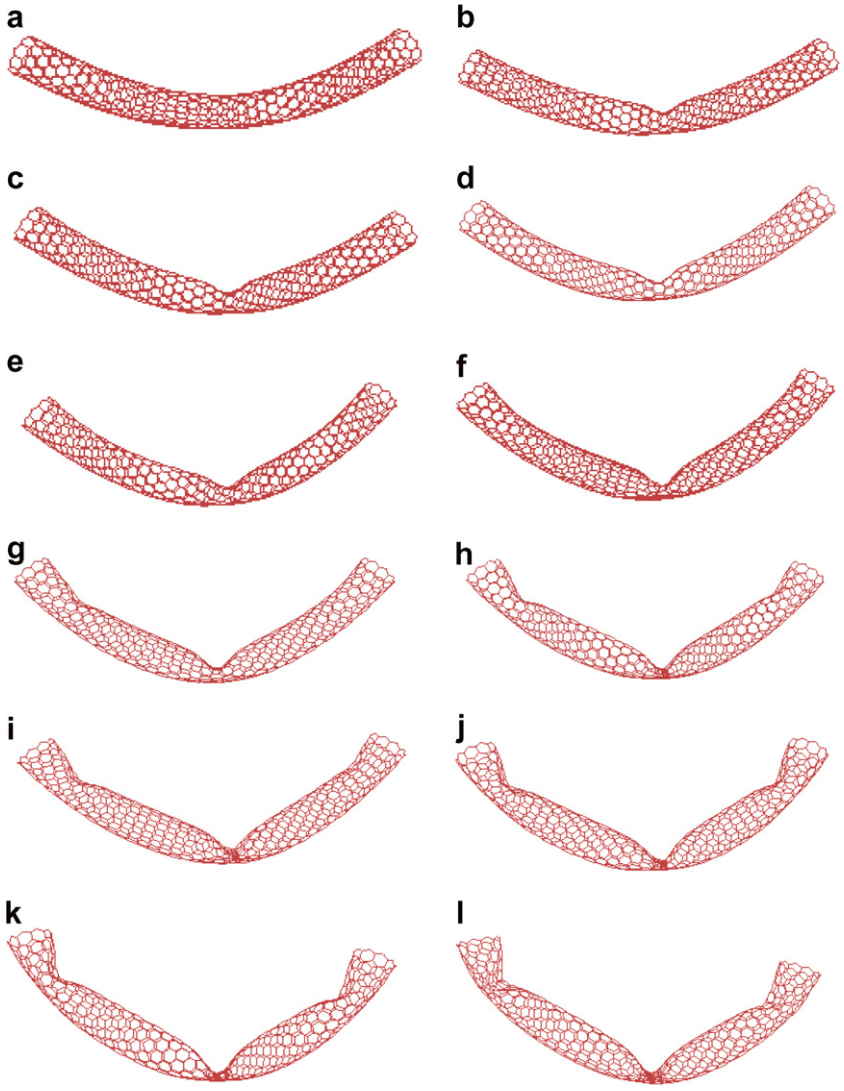

Fig. 5. The morphologies of the (10, 0) SWNT in bending: (a) bending angle of 1.02, (b) bending angle of 1.04, (c) bending angle of 1.20, (d) bending angle of 1.40, (e) bending angle of 1.60, (f) bending angle of 1.80, (g) bending angle of 1.82, (h) bending angle of 1.92, (i) bending angle of 2.00, (j) bending angle of 2.20, (k) bending angle of 2.40 and (l) bending angle of 2.60.

and Iijima et al. [4]. The mechanism of kink initiation as morphological bifurcation of atomistic system, the dependence on the aspect ratio and number of walls, and the prediction on the number of kinks, are still open questions for the future research.

Acknowledgements

A.L. acknowledges the support from Research Grant Council of Hong Kong Grant #1161/05E. Y.H. acknowledges the support from ONR Composites for Marine Structures Program (Grants # N00014-01-1-0205, Program Manager Dr. Y.D.S. Rajapakse).

References

[1] Lourie O, Cox DM, Wagner HD. Buckling and collapse of embedded carbon nanotubes. Phys Rev Lett 1998;81:1638–41.
[2] Hadjiev VG, Lagoudas DC, Oh ES, Thakre P, Davis D, Files BS, et al. Buckling instabilities of octadecylamine functionalized carbon nanotubes embedded in epoxy. Compos Sci Tech 2006;66:128–36.
[3] Yakobson BI, Brabec CJ, Bernholc J. Nanomechanics of carbon tubes: instabilities beyond linear response. Phys Rev Lett 1996;76:2511–4.
[4] Iijima S, Brabec C, Maiti A, Bernholc J. Structural flexibility of carbon nanotubes. J Chem Phys 1996;104:2089–92.
[5] Shibutani Y, Ogata S. Mechanical integrity of carbon nanotubes for bending and torsion. Model Simul Mater Sci Eng 2004;12:599–610.
[6] Liew KM, Wong CH, He XQ, Tan MJ, Meguid SA. Nanomechanics of single and multiwalled carbon nanotubes. Phys Rev B 2004;69:115429.
[7] Liew KM, He XQ, Wong CH. On the study of elastic and plastic properties of multi-walled carbon nanotubes under axial tension using molecular dynamics simulation. Acta Mater 2004;52:2521–7.
[8] Liew KM, Wong CH, Tan MJ. Tensile and compressive properties of carbon nanotube bundles. Acta Mater 2006;54:225–31.
[9] Pantano A, Parks DM, Boyce MC. Mechanics of deformation of single- and multi-wall carbon nanotubes. J Mech Phys Solids 2004;52:789–821.

[10] Wang XY, Wang X. Numerical simulation for bending modulus of carbon nanotubes and some explanations for experiment. Compos: Part B 2004;35:79–86.
[11] Vodenitcharova T, Zhang LC. Mechanism of bending with kinking of a single-walled carbon nanotube. Phys Rev B 2004;69:115410.
[12] Wang Q, Hu T, Chen G, Jiang Q. Bending instability characteristics of double-walled carbon nanotubes. Phys Rev B 2005;71:045403.
[13] Liu B, Huang Y, Jiang H, Qu S, Hwang KC. The atomic-scale finite element method. Comput Meth Appl Mech Eng 2004;193:1849–64.
[14] Liu B, Jiang H, Huang Y, Qu S, Yu MF, Hwang KC. Atomic-scale finite element method in multiscale computation with applications to carbon nanotubes. Phys Rev B 2005;72:035435.
[15] Leung A, Guo X, He XQ, Jiang H, Huang Y. Post-buckling of carbon nanotubes by atomic-scale finite element. J Appl Phys 2006;99:124308.
[16] Brenner DW, Shenderova OA, Harrison JA, Stuart SJ, Ni B, Sinnott SB. A second-generation reactive empirical bond order (rebo) potential energy expression for hydrocarbons. J Phys: Condens Mat 2002;14:783–802.
[17] ABAQUS, ABAQUS Theory Manual and Users Manual, 2002, version 6.2, Hibbit, Karlsson and Sorensen Inc., Pawtucket, RI, USA.
[18] Humphrey W, Dalke A, Schulten K. VMD – visual molecular dynamics. J Mol Graphics 1996;14:33–8.
[19] Falvo MR, Clary GJ, Taylor II RM, Chi Jr V, Brooks FP, Washburn S, et al. Bending and buckling of carbon nanotubes under large strain. Nature (London) 1997;389:582–4.
[20] Demczyk BG, Wang YM, Cumings J, Hetman M, Han W, Zettl A, et al. Direct mechanical measurement of the tensile strength and elastic modulus of multiwall carbon nanotubes. Mater Sci Eng A 2002;334:173–8.
[21] Cao A, Dickrell PL, Sawyer WG, Ghasemi-Nejhad MN, Ajayan PM. Super-compressible foamlike carbon nanotube films. Science 2005;310:1307–10.
[22] Brenner DW. Empirical potential for hydrocarbons for use in simulating the chemical vapor deposition of diamond films. Phys Rev B 1990;42:9458–71.
[23] Arroyo M, Belytschko T. Finite element methods for the non-linear mechanics of crystalline sheets and nanotubes. Int J Numer Meth Eng 2004;59:419–56.